Analyst

PAPER

View Article Online
View Journal | View Issue

Cite this: *Analyst*, 2014, **139**, 4525

A three-dimensional interpenetrating electrode of reduced graphene oxide for selective detection of dopamine†

Xiaowen Yu, Kaixuan Sheng and Gaoquan Shi*

Received 4th April 2014
Accepted 19th June 2014

DOI: 10.1039/c4an00604f

www.rsc.org/analyst

Electrochemical detection of dopamine plays an important role in medical diagnosis. In this paper, we report a three-dimensional (3D) interpenetrating graphene electrode fabricated by electrochemical reduction of graphene oxide for selective detection of dopamine. This electrochemically reduced graphene oxide (ErGO) electrode was used directly without further functionalization or blending with other functional materials. This electrode can efficiently lower the oxidation potential of ascorbic acid; thus, it is able to selectively detect dopamine in the presence of ascorbic acid and uric acid. The ErGO-based biosensor exhibited a linear response towards dopamine in the concentration range of 0.1–10 μM with a low detection limit of 0.1 μM. Furthermore, this electrode has good reproducibility and environmental stability, and can be used to analyse real samples.

1. Introduction

3,4-Dihydroxyphenylethylamine, dopamine (DA), is one of the important neurotransmitters, playing a significant role in the function of human metabolism, cardiovascular, central nervous, renal, and hormonal systems.[1,2] Abnormal levels of DA in body fluids are the indications of many serious diseases such as Schizophrenia, Huntington's and Parkinson's diseases.[3] Electrochemical methods have been extensively explored for the detection of DA because of their simple processes and cheap instruments.[4] However, the major challenge of sensing DA in real samples is the coexistence of high concentrations of ascorbic acid (AA) and uric acid (UA) with oxidation potentials close to that of DA at conventional electrodes offering strong interference.[5,6]

On the other hand, graphene materials have been widely applied for the fabrication of electrochemical sensors because of their unique atom-thick two-dimensional structures, high conductivity and electrocatalytic activities, large specific surface areas and excellent electrochemical stability.[7–15] However, in these cases, graphene sheets were usually coated on the surfaces of substrate electrodes as compact films. As a result, the inherent properties of individual graphene sheets cannot be inherited to the buck graphene coatings.[16] To address this problem, many attempts have been made to construct three-dimensional (3D) graphene architectures.[16–18] These 3D architectures provide graphene materials with high specific surface areas, strong mechanical strength and fast mass and electron transport kinetics because of the combination of 3D porous structures and the excellent intrinsic properties of graphene.[17] One of the most widely used 3D porous graphene materials used for electrochemical sensing was prepared by chemical vapour deposition (CVD) of graphene sheets onto nickel foams.[18] The CVD method can produce high-quality graphene with excellent electrical conductivity,[19] while it suffers from high cost and a complicated process. Furthermore, CVD-graphene has a low content of oxygenated species and structural defects, making its electrocatalytic activity much weaker than that of edge plane pyrolytic graphite (EPPG).[20] This is mainly due to the fact that the oxygenated groups and absorption sites of carbon-based electrodes are important for catalyzing the electrochemical reactions of many analytes.[21,22] Electrochemical deposition is a green, facile, and low cost approach to prepare electroactive materials on the surfaces of electrodes, and the modified electrodes can be directly used in electrochemical devices.[17] Here, we report an ErGO electrode with a 3D interpenetrating microstructure for electrochemically sensing DA. This electrode showed excellent performance towards DA with remarkable selectivity and reproducibility, good stability, and a low detection limit of 0.1 μM.

2. Experimental

2.1 Chemicals

Natural graphite powder (325 mesh) was obtained from Qingdao Huatai lubricant sealing S&T Co. Ltd. (Qingdao, China). Uric acid, dopamine hydrochloride, and ascorbic acid were purchased from Alfa Aesar. Human serum purchased from

Department of Chemistry, Tsinghua University, Beijing 100084, People's Republic of China. E-mail: gshi@tsinghua.edu.cn; Fax: +86-10-62771149; Tel: +86-10-62773743

† Electronic supplementary information (ESI) available: Figures about the electrodes prepared under different conditions, the repeatability and stability of the electrodes. See DOI: 10.1039/c4an00604f

BioDee Company (Beijing, China). All other reagents, including H_2SO_4, HCl, H_2O_2 (30 wt%), $KMnO_4$, $NaNO_3$, $LiClO_4$, $K_3Fe(CN)_6$, $K_4Fe(CN)_6$, K_2HPO_4 and $KH_2PO_4 \cdot 3H_2O$, were of analytical pure grade and bought from the Beijing Chemical Reagent Company (Beijing, China). All chemicals were used as received without further purification. The aqueous solutions were prepared using double distilled water. The 0.1 M phosphate buffer solution (PBS, pH = 7.0) was prepared from K_2HPO_4 and $KH_2PO_4 \cdot 3H_2O$.

Graphene oxide (GO) was synthesized from natural graphite powder by a modified Hummers method,[23] and it was purified by dialysis for one week to remove the remaining metal species. Finally it was centrifuged at 4000 rpm to remove the incompletely oxidized graphite powder.

2.2 Preparation of electrodes

ErGO electrodes were fabricated by electrochemical deposition of rGO sheets on the surface of Au electrodes. Prior to use, Au electrodes (3 mm diameter) were carefully polished with 0.5 and 0.05 μm alumina powder slurries, then washed by sonication successively with water and ethanol for a few minutes. The clean Au electrode was used as the working electrode, a platinum (Pt) foil was applied as the counter electrode and all the potentials were referred to a saturated calomel electrode (SCE). A 6 mg mL^{-1} GO dispersion containing 0.2 M $LiClO_4$ was used as the electrolyte. Electrochemical deposition was carried out at a constant potential of −1.2 V by using a CHI 660D potentiostat-galvanostat (CH Instruments Inc.). During this process, GO sheets were reduced into conductive ErGO as reported in the literature.[24–26] Finally, the ErGO electrodes were washed and immersed in deionized water for 1 h to remove the residual GO absorbed on the electrodes. Before using the ErGO electrodes, they should be immersed in water to maintain their morphology.

2.3 Characterization

The morphology of the ErGO electrode was studied by using a field-emission scanning electron microscope (Sirion-200, Japan). Raman spectra were recorded on a Renishaw Raman microscope with a 514 nm laser. X-ray photoelectron spectra (XPS) were taken out by using an ESCALAB 250 photoelectron spectrometer (ThermoFisher Scientific, USA) with Al Kα (1486.6 eV) as the X-ray source set at 200 W and a pass energy of 30 eV for a high resolution scan. The electrochemical tests were performed on a CHI 660D potentiostat-galvanostat (CH Instruments Inc.) at room temperature. An ErGO electrode, a Pt gauze, and an Ag/AgCl electrode were used as the working, counter, and reference electrodes, respectively. All of the solutions were de-oxygenated by bubbling nitrogen gas for 15 min before electrochemical measurements. For chronocoulometry studies, the initial potential was 0.65 V and the potential was stepped to −0.05 V. The electrochemical impedance spectra were taken out in the frequency range of 0.1 Hz to 100 kHz with 5 mV ac amplitude.

3. Results and discussion

3.1 Characterization of ErGO electrodes

The ErGO electrodes were prepared by electrochemical reduction of 6 mg mL^{-1} GO for 5, 10, 20 or 40 s, and they are denoted as ErGO-t, where t is the time of electrodeposition in seconds. Here, we take ErGO-10 (Fig. S1†) as an example for morphological and structural studies, and its SEM images are shown in Fig. 1. The ErGO sheets generated by electrochemical reduction have more conjugated domains and less oxygenated groups than those of their GO precursor. As a result, upon driving of the electric field, they were self-assembled to form a 3D interpenetrating network (Fig. 1A and B) with a thickness of about 30 μm (Fig. 1C) because of hydrophobic and π-stacking interactions.[27] Furthermore, the residual hydrophilic oxygenated groups of ErGO sheets made the pores of the 3D network become filled with an aqueous electrolyte. The pore sizes of the network are in the range of several micrometers to larger than ten micrometers. The pore walls consist of thin layers of stacked graphene sheets, providing physical cross-linking sites to stabilize the interpenetrating 3D network.[27] The pore walls are nearly vertical to the surface of the Au electrode (Fig. 1B–D); therefore, the micropores in the electrode are fully exposed to the electrolyte for the access of ions and target molecules. Moreover, the upright oriented graphene sheets provide more graphene edges as active sites for electrocatalysis.[28–32]

The Raman spectra of GO or ErGO-10 (Fig. 2A) have two prominent bands around 1340 and 1580 cm^{-1}, and they are assigned to the D- and G-bands of carbon, respectively. The D-band is associated with the structural defects or partially disordered structures of graphite domains and the G-band is related to graphitic carbon.[33] The intensity ratio of D- to G-bands (I_D/I_G) of GO was calculated to be 0.72, while that of ErGO-10 was increased to 1.28. This result indicates that the oxidized areas of GO sheets were partly restored upon reduction to form small conjugated domains.[34]

The C 1s XPS spectra of GO and ErGO-10 (Fig. 2B) indicate the presence of 4 types of carbon bonds: C–C/C=C (284.6 eV), C–O (286.6 eV), C=O (287.8 eV), and O–C=O (289.0 eV).[27] However, in the spectrum of ErGO-10, the bands associated with the oxygenated groups are much weaker than those in the spectrum of GO. The C/O atomic ratio of GO was measured to be 2.27 and that of ErGO-10 was increased to 3.14. These results also confirm that the oxygenated functional groups of GO were partially removed after electrochemical reduction.

3.2 Effects of electrodeposition time on ErGO electrodes

The morphology and electrochemical performances of ErGO electrodes can be modulated by controlling the time of electrodeposition. With increasing the deposition time from 5 to 40 s, the thickness of the ErGO interpenetrating layer increased from about 10 to approximately 50 μm (Fig. 1 and S2†). The cyclic voltammograms (CVs) of the ErGO electrodes in pure PBS are rectangular in shapes and the areas of the rectangles increased with the thickness of the graphene layer (Fig. S3A†). Accordingly, the ErGO electrodes exhibited electrochemical

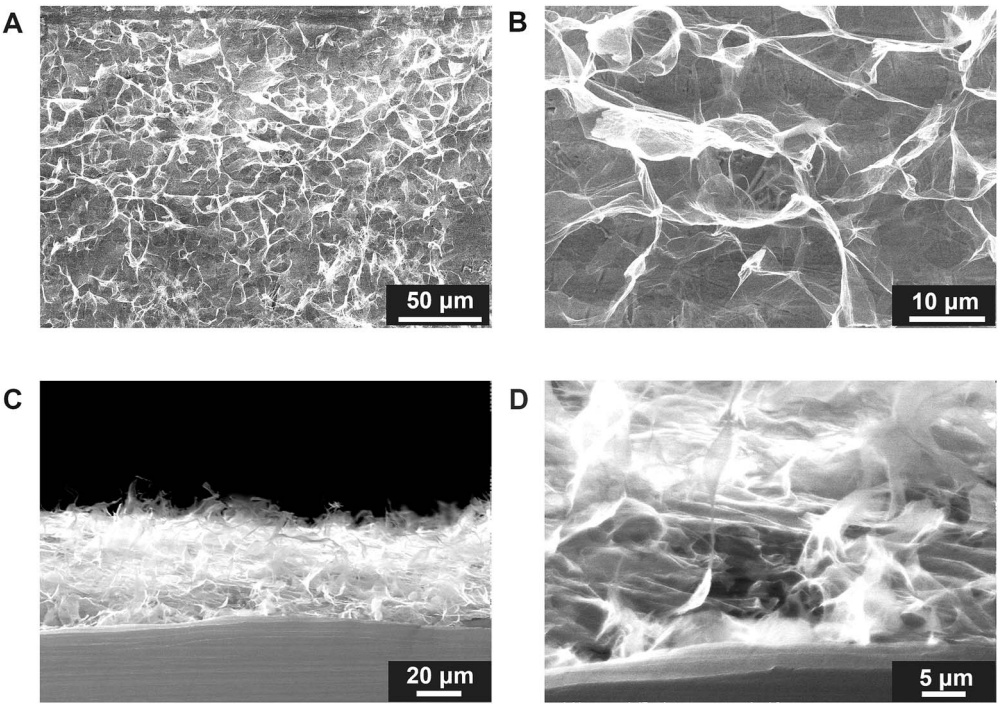

Fig. 1 (A and B) top view and (C and D) cross-sectional scanning electron microscopy images of ErGO-10 deposited on an Au substrate electrode with different magnifications.

double layer behavior and their areal specific capacitances increased with the increase of electrodeposition time.[25] The performances of the ErGO electrodes toward 10 μM DA in PBS were studied by differential pulse voltammetry (DPV). The ErGO electrode prepared by the electrochemical deposition for 10 s (ErGO-10) showed the strongest electrochemical response (Fig. S3B and C†). This is possibly due to its optimized microstructure for electrocatalysis. As the electrochemical deposition time was short (*e.g.* ErGO-5), most graphene sheets laid parallel to the surface of the substrate electrode to form a compact film. However, with the increase in deposition time (*e.g.* ErGO-20 and ErGO-40), the walls of graphene micropores became thicker compared with those of ErGO-10 because of the stacking of graphene sheets. Furthermore, the increase in thickness of the graphene layer also increased the distances of charge transfer and ion diffusion. Thus, we chose an ErGO-10 electrode for the detection of DA.

3.3 Electrochemical behavior of the ErGO-10 electrode

Potassium ferricyanide solution was used to evaluate the electrochemical behavior of the ErGO-10 electrode. Fig. 3A shows the chronocoulometric curve of an ErGO-10 or an Au electrode for the reduction of 1 mM $K_3Fe(CN)_6$ in the aqueous solution of 2 M KCl. The effective surface areas of both electrodes were calculated by the use of the following equation:[35,36]

$$Q = (2nFAD_0^{1/2}\pi^{-1/2}C_0)t^{1/2}$$

where Q is the absolute value of the reduction charge, n is the number of electrons for the reaction (ferricyanide, $n = 1$), F is the Faraday constant (96 485 C mol^{-1}), A is the surface area of the electrode, D_0 is the diffusion coefficient of the oxidized form (ferricyanide, $D_0 = 7.6 \times 10^{-6}$ cm^2 s^{-1}), C_0 is the bulk concentration of the oxidized form (1 mM), and t is the time. According to the slope of the linear plot of Q *versus* $t^{1/2}$, the electrochemically active surface area of the Au electrode was calculated to be 0.070 cm^2, and this value is in consistent with its geometry surface area (0.071 cm^2). The chronocoulometric curve of the ErGO-10 electrode starts at a high charge value because of the high electric double layer capacitance of the electrode, and bends at the initial region caused by the surface adsorption of oxidized species.[35] According to the slope of the linear region of this curve, the electrochemically active surface area of the ErGO-10 electrode was measured to be about twice that of the Au electrode (0.133 cm^2), indicating its improved ability on electrochemical reaction.[36,37]

The capability of electron transfer of the ErGO-10 or the Au electrode was further investigated by AC impedance analysis (Fig. 3B). The Nyquist plot of the bare Au electrode exhibits a semicircle with a charge-transfer resistance (R_{ct}) of about 212 Ω. In comparison, the spectrum of the ErGO-10 electrode is nearly a straight line with a negligible R_{ct}. This is mainly due to the opened porous microstructure of the ErGO-10 electrode that makes nearly all of the graphene sheets accessible to the electrolyte, facilitating the transfer of electrons and the diffusion of ions during the process of electrochemical reaction.

3.4 Electrochemical behaviors of AA, DA, and UA at the ErGO-10 or the Au electrode

Fig. 4 illustrates the CVs of 1 mM AA, DA, or UA at the ErGO-10 or the Au electrode. The CV of AA at a bare Au electrode shows

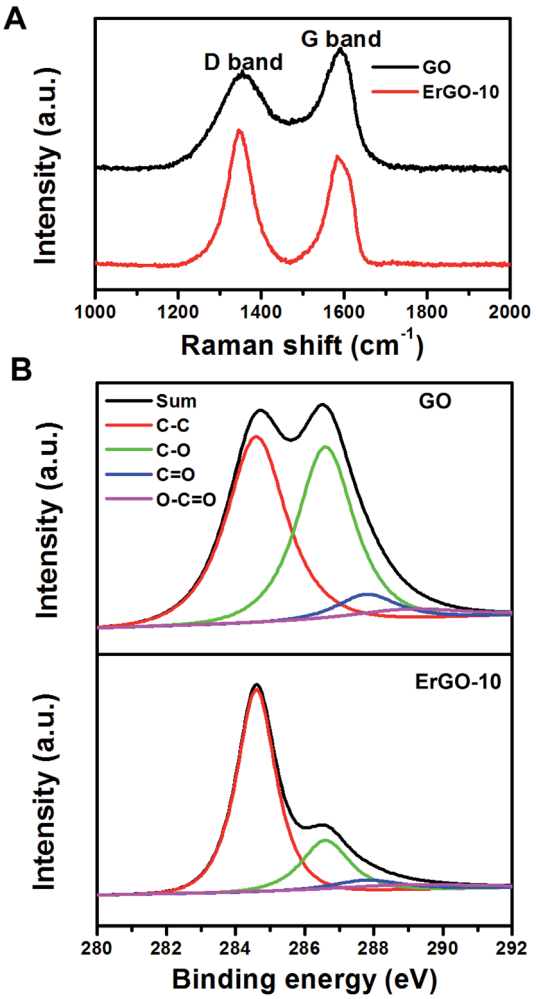

Fig. 2 (A) 514.5 nm excited Raman and (B) C 1s XPS spectra of GO and ErGO-10.

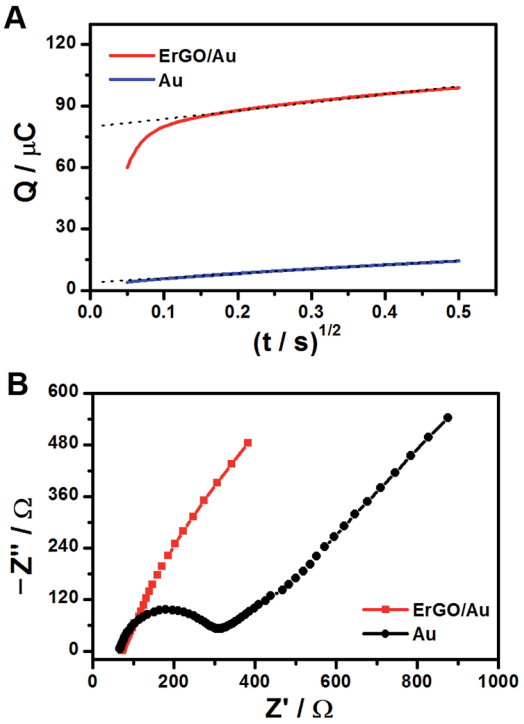

Fig. 3 (A) Chronocoulometric curve for the reduction of 1 mM $K_3Fe(CN)_6$ in 2 M KCl at the ErGO-10 or the Au electrode; (B) Nyquist plots of ErGO-10 and Au electrodes in 5 mM $Fe(CN)_6^{3-/4-}$ containing 0.1 M KCl.

only a broad oxidation wave centered at +0.367 V (Fig. 4A). However, at the ErGO-10 electrode, this wave was negatively shifted for 0.393 V to be centered at around −0.026 V. The negative shift of the peak potential of AA is especially crucial to the separation of three analytes.[38] The CV of DA at the ErGO-10 electrode has a couple of redox waves and the potential difference of their peaks (ΔE_p) was measured to be only 0.043 V, whereas the ΔE_p in the CV at the Au electrode was calculated to be as large as 0.196 V (Fig. 4B). The anodic wave potential at the ErGO-10 electrode is about +0.210 V, lower than that at the Au electrode. In the case of UA (Fig. 4C), a couple of redox waves with a ΔE_p of 0.058 V are observed from the CV at the ErGO-10 electrode. The peak potential of the oxidation wave was measured to be +0.375 V and this value is 0.152 V lower than that observed at the Au electrode (+0.517 V). Furthermore, the current densities of the oxidation waves of AA, DA, and UA at the ErGO-10 electrode are about 2, 6, and 15 times those at the Au electrode, respectively. The large negative shifts of the anodic wave potentials together with the strong enhancements in redox currents and the decrease in ΔE_p indicate the excellent electrocatalytic activity and fast electron transport kinetics at the ErGO-10 electrode.[39,40] The superior performance of the ErGO-10 electrode is attributed to its large electrochemically active area and negligible R_{ct} (Fig. 3) as well as its multiplexed and highly conductive pathways provided by the 3D interpenetrating graphene network.[16,41] Furthermore, the exposed edges of ErGO sheets are favourable sites for transferring electrons from the electrode to biomolecules.[30,31,37,42] In order to demonstrate that the 3D architecture of the ErGO-10 electrode plays a key role in its electrochemical performances, we dried this electrode in air. As a result, the 3D microstructure of ErGO was collapsed to form a compact 2D film because of the volume contraction of the graphene layer and π-stacking of graphene sheets during the process of drying (Fig. S4†). The DPV curve of 1 mM DA at the compact 2D graphene electrode showed an oxidation current density about 3 times weaker than that at the untreated ErGO-10 electrode (Fig. S5†). This is mainly due to the compact 2D ErGO film that has much smaller surface area for the access of the electrolyte and DA molecules and fewer exposed graphene edges for electrocatalysis.

3.5 Simultaneous detection of AA, DA, and UA

AA, DA, and UA coexist in serum and other extracellular body fluids and their selective determination in a ternary mixture is of great importance in biosensing. For this purpose, a mixture of 5 mM AA, 0.1 mM DA, and 0.1 mM UA was used as the sensing sample. The CV of this mixture at the Au electrode shows only a broad oxidation wave in the potential range of

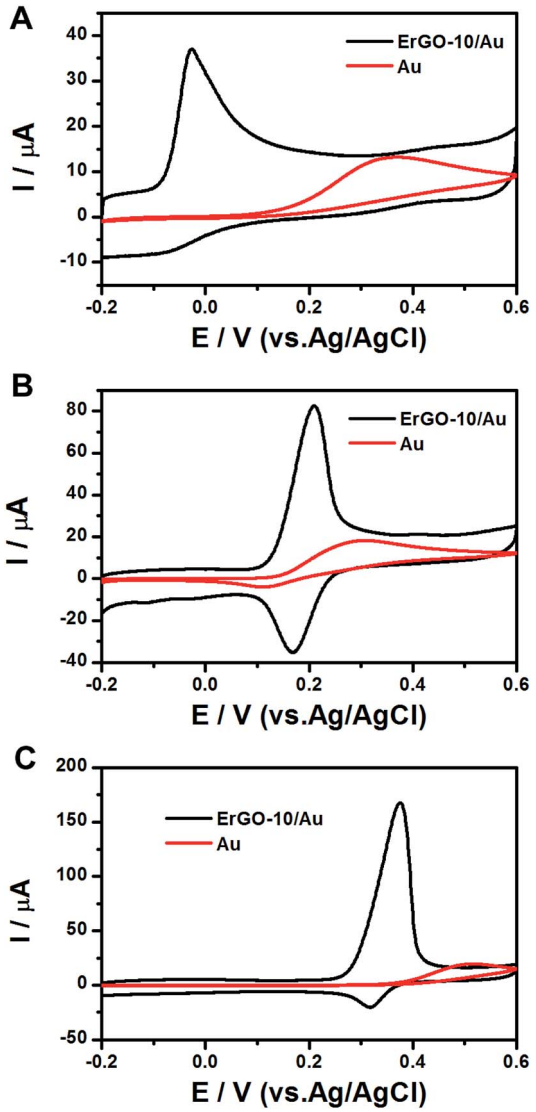

Fig. 4 CVs of 1 mM AA (A), DA (B), and UA (C) at the ErGO-10 or the Au electrode. Electrolyte = 0.1 M PBS, pH 7.0; scan rate = 50 mV s^{-1}.

0.1 to 0.6 V because of the wave overlapping of the three analytes (Fig. 5A). In comparison, at the ErGO-10 electrode, the CV shows three well-defined peaks at approximately −0.013 (AA), +0.197 (DA) and +0.336 V (UA), respectively. The peak potential separations between neighboring waves were measured to be 0.210 V (AA and DA) and 0.139 V (DA and UA). Accordingly, the ErGO-10 electrode can provide much larger voltammetric peak separations than those of the Au electrode; thus, it can efficiently detect one species in the presence of other two coexist analytes. The selectivity of our ErGO-10 electrode is superior to that of the electrode based on multilayer graphene nanoflakes[32] or functionalized graphene.[43] It should be noted here that the reduction waves of these three analytes are also shown in the CV curve of the ErGO-10 electrode, reflecting the ultrahigh electrocatalytic activity of this electrode. In addition, the ErGO-10 electrode can also discriminate these three species even at a fast scan rate of 1000 mV s^{-1} (Fig. S6†). This is possibly due to the high efficiency of electron transfer between the molecules of analytes and the 3D interpenetrating graphene network of the ErGO-10 electrode.

DPV analysis also exhibited excellent performance in simultaneous determination of AA, DA, and UA without any interference. As shown in Fig. 5B, the oxidation peaks of 5 mM AA, 0.1 mM DA, and 0.1 mM UA at the ErGO-10 electrode are centered at −0.076, +0.164, and +0.296 V, respectively. The potential separations among the peaks are 0.240 (AA and DA), 0.132 (DA and UA), and 0.372 V (AA and UA), larger than the values achieved at a chitosan–graphene modified electrode (correspondingly, 0.165, 0.090, and 0.255 V).[44] These results also reflect that the ErGO-10 electrode can be used for simultaneous sensing of these three species in a mixture. It should be noted here that ErGO-10 was used directly without further functionalization or blending with other functional materials.

Fig. 5C illustrates the DPV curves of DA with different concentrations at the ErGO-10 electrode in the presence of 500 μM AA and 10 μM UA. The peak current of the DPV curve increases linearly with the concentration of DA in the range of 1 to 100 μM (Fig. 5D), indicating that the interference of AA and UA is negligible.

3.6 Amperometric response of DA

The amperometric responses of the ErGO-10 electrode towards DA at +0.200 V are demonstrated in Fig. 6. Fig. 6A shows an amperometric current–time plot and the limit of detection was tested to be as low as 0.1 μM ($S/N = 3$), and the corresponding calibration curve is the inset of the figure. This value is lower than those reported previously for the graphene modified electrodes (≥0.5 μM).[43–47] In Fig. 6B, the linear relationship between the peak currents and DA concentrations was obtained for the DA range of 0.1–10 μM. The linear regression equation is I (μA) = 0.0443C (μM), with a correlation coefficient of R = 0.9996 ($N = 3$), where I and C are the current of response and the concentration of DA.

3.7 Reproducibility and stability of the ErGO-10 electrode

The reproducibility of the ErGO-10 electrode was investigated by using 6 electrodes prepared under identical conditions, and the relative standard deviation (RSD) of their electrochemical responses to 1 mM DA was measured to be only 1.4% (Fig. S7†). The amperometric response remained 88% of its initial value after immersing for 1500 s in the solution of 50 μM DA under stirring (Fig. S8†). The ErGO-10 electrode also showed excellent environmental stability; it retained about 90% of its initial current signal after storing in PBS at 4 °C for 1 week (Fig. S9†).

3.8 Real sample analysis

The detection of DA in human serum was also performed to clarify whether the ErGO-10 electrode can be practically applied for analyzing real samples. For this purpose, human serum was first centrifuged at 4000 rpm for 20 min to obtain a transparent liquid outside the ultrafiltration membrane (molecular weight cut off = 5 kDa). Then, the purified serum was diluted ten times (by volume) with PBS. Diluted human serum containing 10 μM DA was measured by DPV with the ErGO-10 electrode and the

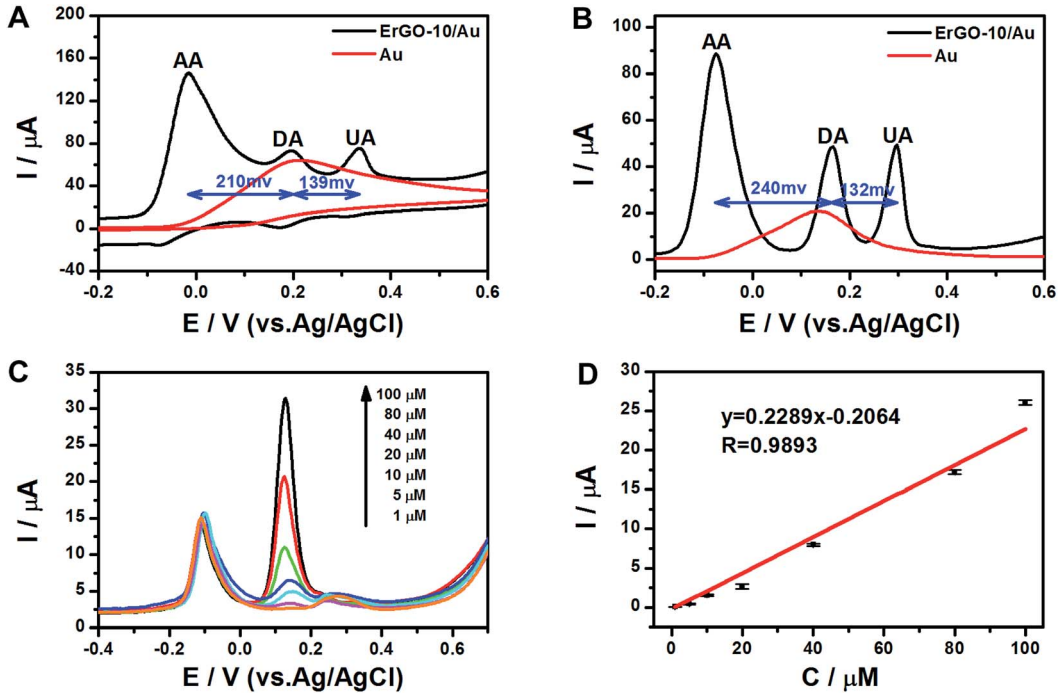

Fig. 5 (A) CVs (scan rate: 50 mV s^{-1}) and (B) DPVs (pulse width: 0.2 s; pulse period: 0.5 s) of a mixed solution containing 5 mM AA, 0.1 mM DA, and 0.1 mM UA at the ErGO-10 or the Au electrode. (C) DPVs of a 0.1 M pH 7.0 PBS solution containing 500 μM AA, 10 μM UA and different concentrations of DA at the ErGO-10 electrode. (D) Linear fit of peak currents to concentrations of DA according to the curves shown in panel C.

measurements were repeated 5 times (Fig. S10†). The found values were calculated by referring to the standard curve shown in Fig. 5D (Table 1). Accordingly, the average recovery was calculated to be 99.70% with a relative standard derivation of only 2.22%. These results reflect that the substrates in serum (*e.g.* AA, UA, proteins, and amino acids) do not interfere the detection of DA, suggesting that the ErGO-10 electrode can be applied for analyzing real samples.

Table 1 Electrochemical detection of 10 μM DA in human serum for 5 times with ErGO-10 electrodes

Sample	Found (μM)	Recovery (%)
1	9.94	99.4
2	9.71	97.1
3	10.17	101.7
4	10.22	102.2
5	9.81	98.1

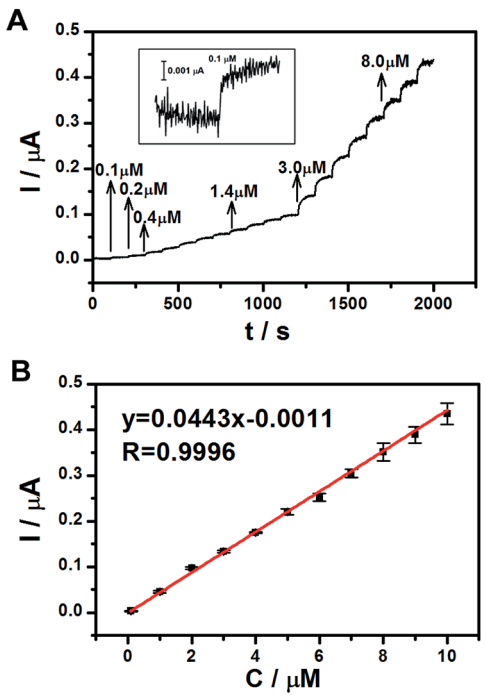

Fig. 6 (A) Amperometric responses of the ErGO-10 electrode at 0.200 V after the subsequent addition of DA in a 0.1 M PBS (pH 7.0) solution; the inset is the corresponding calibration curve of 0.1 μM DA. (B) Linear fit of peak currents to the concentrations of DA.

4. Conclusions

We developed a one-step electrochemical method to fabricate a 3D interpenetrating ErGO electrode for electrochemical sensing. This method, analogous to the electroplating process, can be carried out in an aqueous medium and does not need expensive equipment like the CVD technique or a toxic reducing agent frequently required by chemical reduction of GO. Therefore, it is fast, simple, cheap, eco-friendly, easy controllable, and readily scalable to industrial levels. Furthermore, the microporous 3D ErGO electrode has high electrochemical performance because of its large accessible surface area, highly conductive

channels and strong electrocatalytic activity. Therefore, it can be used to selectively detect DA with an extremely low limit of detection compared with other graphene electrodes. The ErGO electrode can be used directly without further modification or blending with other functional materials. The 3D interpenetrating ErGO electrode provides a promising and attractive platform for fabricating electrochemical biosensors with good selectivity, sensitivity, reproducibility, and stability.

Acknowledgements

This work was supported by the National Basic Research Program of China (2012CB933402) and the National Natural Science Foundation of China (51161120361 and 21274074).

Notes and references

1 J. F. van Staden and R. I. van Staden, *Talanta*, 2012, **102**, 34.
2 M. L. Heien, A. S. Khan, J. L. Ariansen, J. F. Cheer, P. E. Phillips, K. M. Wassum and R. M. Wightman, *Proc. Natl. Acad. Sci.*, 2005, **102**, 10023.
3 R. M. Wightman, L. J. May and A. C. Michael, *Anal. Chem.*, 1988, **60**, 769A.
4 P. Quan do, P. Tuyen do, T. D. Lam, P. T. Tram, N. H. Binh and P. H. Viet, *Colloids Surf., B*, 2011, **88**, 764.
5 C. Deng, J. Chen, M. Wang, C. Xiao, Z. Nie and S. Yao, *Biosens. Bioelectron.*, 2009, **24**, 2091.
6 M. Bagherzadeh and M. Heydari, *Analyst*, 2013, **138**, 6044.
7 A. K. Geim and K. S. Novoselov, *Nat. Mater.*, 2007, **6**, 183.
8 R. M. Westervelt, *Science*, 2008, **320**, 324.
9 D. A. C. Brownson and C. E. Banks, *Analyst*, 2010, **135**, 2768.
10 Y. Liu, X. Dong and P. Chen, *Chem. Soc. Rev.*, 2012, **41**, 2283.
11 C. Huang, C. Li and G. Shi, *Energy Environ. Sci.*, 2012, **5**, 8848.
12 D. Chen, L. Tang and J. Li, *Chem. Soc. Rev.*, 2010, **39**, 3157.
13 S. Alwarappan, A. Erdem, C. Liu and C.-Z. Li, *J. Phys. Chem. C*, 2009, **113**, 8853.
14 S. Alwarappan, C. Liu, A. Kumar and C.-Z. Li, *J. Phys. Chem. C*, 2010, **114**, 12920.
15 M. Mishra, S. Alwarappan, R. K. Joshi and T. Mohanty, *J. Nanosci. Nanotechnol.*, 2013, **13**, 4040.
16 X. Dong, X. Wang, L. Wang, H. Song, H. Zhang, W. Huang and P. Chen, *ACS Appl. Mater. Interfaces*, 2012, **4**, 3129.
17 C. Li and G. Shi, *Nanoscale*, 2012, **4**, 5549.
18 D. A. C. Brownson, L. C. S. Figueiredo-Filho, X. Ji, M. Gomez-Mingot, J. Iniesta, O. Fatibello-Filho, D. K. Kampouris and C. E. Banks, *J. Mater. Chem. A*, 2013, **1**, 5962.
19 X. Cao, Y. Shi, W. Shi, G. Lu, X. Huang, Q. Yan, Q. Zhang and H. Zhang, *Small*, 2011, **7**, 3163.
20 D. A. C. Brownson, M. Gomez-Mingot and C. E. Banks, *Phys. Chem. Chem. Phys.*, 2011, **13**, 20284.
21 D. A. C. Brownson, R. V. Gorbachev, S. J. Haigh and C. E. Banks, *Analyst*, 2012, **137**, 833.
22 D. A. C. Brownson, C. W. Foster and C. E. Banks, *Analyst*, 2012, **137**, 1815.
23 W. S. Hummers and R. E. Offeman, *J. Am. Chem. Soc.*, 1958, **80**, 1339.
24 M. Hilder, B. Winther-Jensen, D. Li, M. Forsyth and D. R. MacFarlane, *Phys. Chem. Chem. Phys.*, 2011, **13**, 9187.
25 K. Sheng, Y. Sun, C. Li, W. Yuan and G. Shi, *Sci. Rep.*, 2012, **2**, 247.
26 Y. Li, K. Sheng, W. Yuan and G. Shi, *Chem. Commun.*, 2013, **49**, 291.
27 Y. Xu, K. Sheng, C. Li and G. Shi, *ACS Nano*, 2010, **4**, 4324.
28 C. Gómez-Navarro, J. C. Meyer, R. S. Sundaram, A. Chuvilin, S. Kurasch, M. Burghard, K. Kern and U. Kaiser, *Nano Lett.*, 2010, **10**, 1144.
29 K. Erickson, R. Erni, Z. Lee, N. Alem, W. Gannett and A. Zettl, *Adv. Mater.*, 2010, **22**, 4467.
30 C. E. Banks and R. G. Compton, *Analyst*, 2005, **130**, 1232.
31 C. E. Banks, T. J. Davies, G. G. Wildgoose and R. G. Compton, *Chem. Commun.*, 2005, 829.
32 N. G. Shang, P. Papakonstantinou, M. McMullan, M. Chu, A. Stamboulis, A. Potenza, S. S. Dhesi and H. Marchetto, *Adv. Funct. Mater.*, 2008, **18**, 3506.
33 K. N. Kudin, B. Ozbas, H. C. Schniepp, R. K. Prud'homme, I. A. Aksay and R. Car, *Nano Lett.*, 2008, **8**, 36.
34 A. C. Ferrari and J. Robertson, *Phys. Rev. B: Condens. Matter Mater. Phys.*, 2000, **61**, 14095.
35 A. J. Bard and L. R. Faulkner, *Electrochemical Methods, Fundamentals and Applications*, John Wiley and Sons, Beijing, 2nd ed. 2005.
36 M. Csiszar, A. Szucs, M. Tolgyesi, A. Mechler, J. B. Nagy and M. Novak, *J. Electroanal. Chem.*, 2001, **497**, 69.
37 M. Zhou, Y. Zhai and S. Dong, *Anal. Chem.*, 2009, **81**, 5603.
38 C.-L. Sun, H.-H. Lee, J.-M. Yang and C.-C. Wu, *Biosens. Bioelectron.*, 2011, **26**, 3450.
39 Y. Guo, S. Guo, J. Ren, Y. Zhai, S. Dong and E. Wang, *ACS Nano*, 2010, **4**, 4001.
40 C.-L. Sun, C.-T. Chang, H.-H. Lee, J. Zhou, J. Wang, T.-K. Sham and W.-F. Pong, *ACS Nano*, 2011, **5**, 7788.
41 R. S. Kelly, D. J. Weiss, S. H. Chong and T. Kuwana, *Anal. Chem.*, 1999, **71**, 413.
42 W. Yuan, Y. Zhou, Y. Li, C. Li, H. Peng, J. Zhang, Z. Liu, L. Dai and G. Shi, *Sci. Rep.*, 2013, **3**, 2248.
43 M. Mallesha, R. Manjunatha, C. Nethravathi, G. S. Suresh, M. Rajamathi, J. S. Melo and T. V. Venkatesha, *Bioelectrochemistry*, 2011, **81**, 104.
44 D. Han, T. Han, C. Shan, A. Ivaska and L. Niu, *Electroanalysis*, 2010, **22**, 2001.
45 X. Ma, M. Chao and Z. Wang, *Anal. Methods*, 2012, **4**, 1687.
46 Y.-R. Kim, S. Bong, Y.-J. Kang, Y. Yang, R. K. Mahajan, J. S. Kim and H. Kim, *Biosens. Bioelectron.*, 2010, **25**, 2366.
47 Y. Wang, Y. Li, L. Tang, J. Lu and J. Li, *Electrochem. Commun.*, 2009, **11**, 889.